

Spectral hole burning and optically detected nuclear quadrupole resonance in flux-grown stoichiometric europium vanadate crystals

P. C. Hansen, M. J. M. Leask, and B. M. Wanklyn
Clarendon Laboratory, Parks Road, Oxford OX1 3PU, United Kingdom

Y. Sun and R. L. Cone
Physics Department, Montana State University, Bozeman, Montana 59717

M. M. Abraham
Oak Ridge National Laboratory, Oak Ridge, Tennessee 37831

(Received 10 March 1997)

Earlier work [Cone *et al.*, J. Phys. C **17**, 3101 (1984); Cone *et al.*, J. Phys.: Condens. Matter **5**, 573 (1993)] on EuVO_4 has described the fluorescence excitation spectra associated with the large number of defect sites (>50) previously discovered in this material. To establish which if any of the defect sites were intrinsic to the EuVO_4 crystal structure rather than being dependent on particular growth procedures, EuVO_4 crystals were prepared from fluxes with different compositions. The present work extends this study, using the techniques of spectral hole burning and optical detection of nuclear quadrupole resonance to examine at much higher precision the degree to which the defect spectra associated with the various crystal growths are identical, and to attempt a preliminary correlation of such spectra with the methods of crystal growth. We discuss the relative importance of the lattice and electronic contributions to the ground-state quadrupole interactions and conclude that the electronic contribution is almost always larger than the lattice contribution. The data also allow conclusions to be drawn regarding the relative importance of *pseudoquadrupolar* effects in the spectra and they are found to be small. This work forms a basis for detailed study of particular defect sites to be discussed in further papers. [S0163-1829(97)02237-6]

I. INTRODUCTION

In the earliest spectroscopic study of stoichiometric europium vanadate, EuVO_4 ,¹ spectral hole burning techniques were used to investigate crystallographically perturbed defect sites in optically-clear single crystals. Fluorescence excitation spectra in the Eu^{3+} : 7F_0 - 5D_0 region (582 nm) showed more than fifty absorption lines spread over 50–60 cm^{-1} . Each of these lines could be ascribed to a distinct type of defect site in the crystal, since the optical transition in question, being $J=0 \rightarrow J=0$, has no crystal-field splittings associated with either the initial or final state.

This work prompted first a parallel study of the isomorphous compound europium arsenate, EuAsO_4 ,² that showed very similar effects, and second a study of the extent to which the detailed procedures of EuVO_4 crystal growth were determining the observed Eu^{3+} spectra.³ For convenience, Table I here is reproduced and expanded from the latter work. It was observed that the excitation maps for the various EuVO_4 growths are as remarkable for their differences as for their similarities. The main features are as follows.

(1) The frequency of the *intrinsic* transition—due to Eu^{3+} ions at the expected stoichiometric high-symmetry D_{2d} crystal sites—is accurately the same for all growths: 515 544 GHz (17 196.7 cm^{-1}) and could be observed only in applied magnetic field since the ${}^7F_0 \rightarrow {}^5D_0$ transition is strictly forbidden in D_{2d} symmetry in zero magnetic field.

(2) There is an obvious clustering of defect site transitions around the transition for the *intrinsic* site. These are perhaps

mostly “minimally-perturbed” sites. However, apart from a few common features—for instance, the ~ 30 GHz gap in all the spectra just below the *intrinsic* site transition—the spectra for different growths differ markedly in detail.

(3) The spectra for the highest purity samples showed no lines on the high frequency side of 516 200 GHz (17 218 cm^{-1}). For all the other samples, where the crystals had been grown in a flux containing various amounts of fluorine in the form of potassium fluoride, KF, there was a universal appearance of two high energy lines at ~ 516 389 and 516 635 GHz (17 224.88 and 17 233.09 cm^{-1} , respectively), with the former appearing as two lines for some growths.

(4) Zeeman effect studies showed that for the highest energy defects—some 10% of the total number—a magnetic field applied along the crystallographic a, a' axis showed *site-inequivalence* splittings in addition to the expected quadratic Zeeman effect. This was discussed as a consequence of low defect site symmetry, and implied crystal-field splittings in the first excited 7F_1 multiplet of some hundreds of cm^{-1} . These large splittings are in sharp contrast to the 10.2 cm^{-1} crystal-field splitting measured for 7F_1 on the *intrinsic* site.

The work reported here uses *spectral hole burning* (SHB) and *optically detected nuclear quadrupole resonance* (ODNQR) to extend the earlier work to much higher resolution in the frequency domain. All of the spectral lines recorded in the earlier work³—some 600 lines in total—have been investigated by SHB techniques. This survey was designed to determine first whether lines that appear at identi-

TABLE I. Various crystal growths and their fluxes. The europium was added stoichiometrically as an oxide (Eu_2O_3).

Growth	Flux composition	Comments
A: EuVO_4	V_2O_5	Pure
B: EuVO_4	V_2O_5	Superpure
C: $\text{EuVO}_4:0.01\% \text{Gd}^{3+}$	$\text{V}_2\text{O}_5/\text{Gd}_2\text{O}_3$	IBM growth
D: EuVO_4	$\text{Pb}_2\text{V}_2\text{O}_7/\text{V}_2\text{O}_5$	Original growth
E: $\text{GdVO}_4:1\% \text{Eu}^{3+}$	$\text{Pb}_2\text{V}_2\text{O}_7/\text{V}_2\text{O}_5$	For comparison
F: $\text{YVO}_4:10\% \text{Eu}^{3+}$	$\text{Pb}_2\text{V}_2\text{O}_7/\text{V}_2\text{O}_5$	For comparison
G: EuVO_4	$\text{PbO}/\text{PbF}_2/\text{V}_2\text{O}_5$	Excess Pb
H: $\text{EuVO}_4:1.5\% \text{Sm}^{3+}$	$\text{PbO}/\text{PbF}_2/\text{V}_2\text{O}_5/\text{SmO}_3$	Doped with Sm^{3+}
I: EuVO_4	$\text{KF}/\text{V}_2\text{O}_5$	New flux mixture
J: $\text{EuVO}_4:1\% \text{Ho}^{3+}$	$\text{KF}/\text{V}_2\text{O}_5/\text{Ho}_2\text{O}_3$	Doped with Ho^{3+}
K: $\text{EuVO}_4:1\% \text{Dy}^{3+}$	$\text{KF}/\text{V}_2\text{O}_5/\text{Dy}_2\text{O}_3$	Doped with Dy^{3+}
L: EuVO_4	$\text{K}_2\text{O}/\text{V}_2\text{O}_5$	New flux mixture
ORNL	$\text{PbO}/\text{V}_2\text{O}_5$	Oak Ridge National Lab

cal frequencies, though from different EuVO_4 growths, are still identical when viewed through the ‘‘frequency microscope’’ of hole burning. In addition, the rates of hole burning and hole relaxation can be correlated with the presence of paramagnetic impurities that affect Eu^{3+} nuclear spin relaxation in EuVO_4 . A number of lines display very detailed spectra; two of these have already been studied using ODNQR.⁴ Finally, in addition to results for the various crystal growths produced earlier,^{3,4} this work includes the study of crystals grown in a different laboratory (Oak Ridge National Laboratory) as a further test of the universality of the observed defect spectra. As will be seen, the more recent crystal growths are identical to the earlier growths in many, but not all, respects.

II. EXPERIMENTAL METHODS

All experiments were carried out using optically-clear flux-grown EuVO_4 single crystals immersed in superfluid helium at around 1.5 K. For details of crystal growth the reader is referred to the previous paper.³ The techniques of spectral hole burning are well known; since the pioneering work of Erickson,^{5–7} many studies applied to europium and other rare earth compounds have been published.⁸ Hole burning relies upon a selective population redistribution mechanism to bring about long-lived changes in the absorption profile of a spectroscopic line; in rare earth compounds the hyperfine optical pumping mechanism depends on the ion of interest having a nuclear spin $I \geq 1$, with consequent nuclear hyperfine splittings that are inevitably smaller than the inhomogeneous optical linewidth but much larger than the linewidth of a narrow band tunable laser and the homogeneous linewidth of the optical transition.

In the present work the crystal was subjected to cw excitation at modest power levels (~ 15 mW focussed dye laser output), and typical holes burned to the baseline (i.e., total bleaching) in a time ~ 1 s or less, and exhibited a lifetime ≥ 1 h. It is against this experimental procedure that the terms ‘‘easy’’ or ‘‘difficult to burn’’ used below should be judged. The holes were read out with the same laser power and with a 2 GHz/s sweep rate for the typical 0.5–1 GHz scan.

For the Eu^{3+} ion the hyperfine splittings arise primarily from nuclear quadrupole interaction, since first-order effects of the magnetic hyperfine interaction are zero for the $J=0$ electronic angular momentum ground state. There are several possible contributions to effects describable as quadrupole interaction, all occurring in the literature in a variety of operator formalisms, so Appendix A presents a unified account of the theoretical understanding of nuclear quadrupole interaction. The manner in which the experimental hole burning data were analyzed is briefly described in Appendix B.

III. THE QUADRUPOLE INTERACTION HAMILTONIAN

Appendix A gives a full derivation of the effective-spin Hamiltonian

$$H = -\mathbf{B} \cdot \boldsymbol{\gamma} \cdot \mathbf{I} + P \left\{ I_z^2 - \frac{I(I+1)}{3} + \frac{\eta}{6} (I_+^2 + I_-^2) \right\},$$

together with the various contributions to both P and η . For both 5D_0 and 7F_0 the major contributions to P are first P_{latt} , which derives from the crystal lattice, and second P_{4f}^2 , which is the second-order effect due to the $4f$ electrons (first-order effects being zero in $J=0$ states). Both these terms depend on the crystal field parameter B_0^2 and are calculable using the expressions in Appendix A. The results of these calculations are

Excited state:

$${}^5D_0 \text{ total } P = -7.4 \times 10^{-2} B_0^2 \text{ MHz.}$$

$$\text{Ratio } P_{\text{latt}}/P_{4f}^2 = -29,$$

Ground state:

$${}^7F_0 \text{ total } P = -3.4 \times 10^{-2} B_0^2 \text{ MHz.}$$

$$\text{Ratio } P_{\text{latt}}/P_{4f}^2 = -1.8.$$

These results show that $|P({}^5D_0)| > |P({}^7F_0)|$. This is consistent with both the present and previously published data on Eu^{3+} ions in crystals. Also, the lattice contribution, P_{latt}

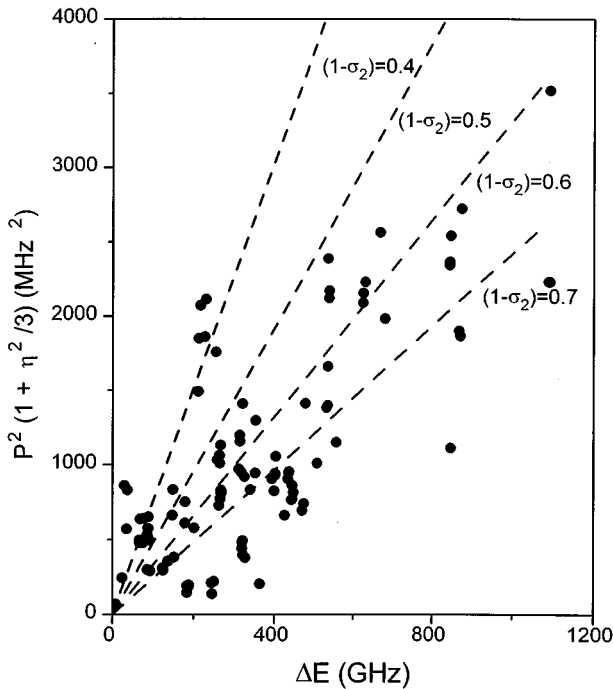


FIG. 1. A plot for 5D_0 of δE vs $P^2(1 + \eta^2/3)$ for 94 defect sites, where P and η correspond to ${}^{153}\text{Eu}:{}^5D_0$, and δE is the energy difference (GHz) between the defect and intrinsic site 7F_0 - 5D_0 transitions. Theoretical predictions based on a range of values for the Sternheimer shielding factor $(1 - \sigma_2)$ are shown for comparison. The best fit to the data is given by $(1 - \sigma_2) = 0.66$. It should be noted that the scatter is not due to a lack of precision in the data: the values of P , η , and δE are all determined with an accuracy of $\sim 1\%$.

dominates $P({}^5D_0)$ but not $P({}^7F_0)$, which has several consequences for the data reported here.

From the hole burning experiments we determine the values of P and the asymmetry parameter η needed to fit the quadrupole Hamiltonian for each of the two europium isotopes ${}^{151}\text{Eu}$ and ${}^{153}\text{Eu}$. If the quadrupole parameter P is determined principally by the sum of P_{latt} and P_{4f}^2 , the ratio $P({}^{151}\text{Eu})/P({}^{153}\text{Eu})$ should be equal to the ratio of their respective quadrupole moments (2.54). Departures from this ratio would be evidence that pseudoquadrupole interactions are significant. The 5D_0 data show little if any departure from the 2.54 ratio, implying that the lattice contribution to P is dominant, as expected. Even the 7F_0 ODNQR data given below, which might have been expected to be more sensitive to pseudoquadrupolar contributions to P , show little departure from this ratio.

IV. HOLE BURNING EXPERIMENTS IN ZERO MAGNETIC FIELD

A total of 94 sets of (P, η) data for the 5D_0 excited state were obtained from the hole burning spectra. All the lines observed in the excitation spectra for the growths A , D , G , I , J , and L (see Table I) were studied; for each growth some 15–20 lines produced analyzable spectra. Some of these 5D_0 results are listed in Table II.

We observed in earlier work on EuAsO_4 (Ref. 2) that the

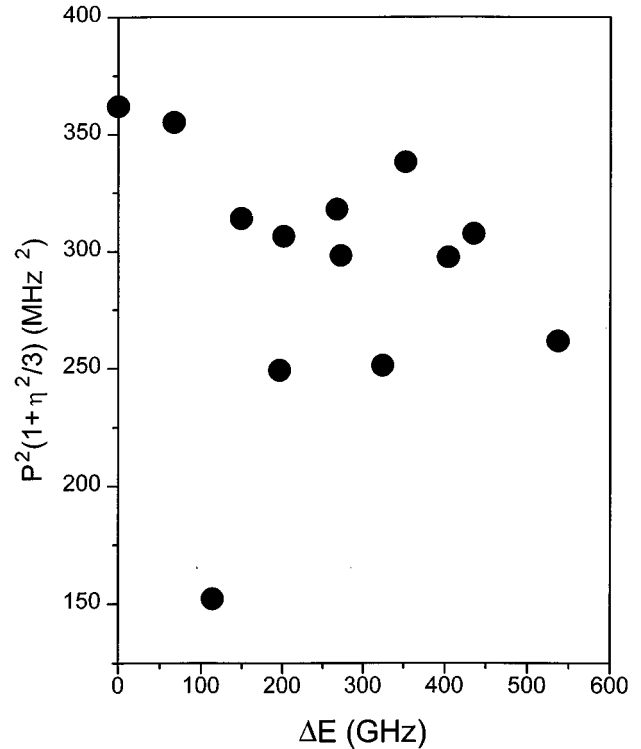


FIG. 2. A plot for 7F_0 of δE vs $P^2(1 + \eta^2/3)$ for the defect sites listed in Table II, where P and η correspond to ${}^{153}\text{Eu}:{}^7F_0$, and δE is the energy difference (GHz) between the defect and intrinsic site 7F_0 - 5D_0 transitions. No obvious functional dependence is evident. It should be noted that the scatter is not due to a lack of precision in the data. The P and η values are determined with an accuracy of 0.1% or better, due to the higher accuracy of the ODNQR experiments.

magnitude of P tends to be larger when the energy difference δE between the defect site and the intrinsic site is larger. This was interpreted hypothetically in terms of crystallographic distortion at each particular defect site and a consequent correlation of P and the rank two crystal field terms with the energy shift caused by these terms. For EuVO_4 , this correlation would be expressed as

$$\delta E = 0.21(1 + \eta^2/3)P^2 \text{ GHz.}$$

Previous analysis for EuAsO_4 indicated a reasonable relationship between δE and P . Here we examined many more sites (94, rather than 11) and thus provide a better test of the model. It must be recognized that each defect site is a highly individual situation and that no simple mathematical treatment of the measured parameters (P, η) in terms of δE is likely to produce a convincing functional variation for all of the data. Figure 1 shows the data compared with the predicted result. Indeed, there is considerable scatter. The best fit to the data is not good, as it corresponds to $(1 - \sigma_2) = 0.66$, which is outside the limit implied by the published value: $(1 - \sigma_2) = 0.5 \pm 0.1$. It should be noted that the scatter in Fig. 1 is not due to experimental error, since the values of P and η are measured to an accuracy of order 1%. As a comparison, Fig. 2 shows the corresponding plot of the (P, η) data for the *ground state* 7F_0 . (These data are listed in Table II and were derived from the ODNQR experiments

TABLE II. Hole burning and ODNQR results on the EuVO_4 ground and excited states. P is the quadrupole interaction parameter (MHz), η is the asymmetry parameter, and δE is the energy difference (GHz) between the defect and intrinsic site 7F_0 - 5D_0 transitions.

Isotopes	Growth A crystal 7F_0 ODNQR				ORNL crystal 7F_0 ODNQR				Growth A crystal 5D_0 SHB			
	Freq. (GHz)	P (MHz)	η	P ratio	Freq. (GHz)	P (MHz)	η	P ratio	Freq. (GHz)	P (MHz)	η	δE (GHz)
${}^{151}\text{Eu}$	516 081	6.12	0.386	2.585	516 084	6.117	0.3855	2.589	516 082	16.9	0.31	537
${}^{153}\text{Eu}$		15.82	0.371			15.83	0.3719					
${}^{151}\text{Eu}$	515 979	6.784	0.408	2.516	515 979	6.7895	0.4084		515 980	10.2	0.81	435
${}^{153}\text{Eu}$		17.07	0.408						25.8	0.81		
${}^{151}\text{Eu}$	515 948	6.02	0.891	2.570								404
${}^{153}\text{Eu}$		15.47	0.854									
${}^{151}\text{Eu}$	515 896	7.05	0.293	2.573								352
${}^{153}\text{Eu}$		18.14	0.289									
${}^{151}\text{Eu}$	515 868	6.135	0.315	2.536	515 868	6.1429	0.3152	2.535	515 865			324
${}^{153}\text{Eu}$		15.56	0.337			15.57	0.3374			17.9	0.85	
${}^{151}\text{Eu}$	515 816	6.543	0.457	2.558	515 810	6.5397	0.4548		515 811			267
${}^{153}\text{Eu}$		16.74	0.438							27.6	0.44	
${}^{151}\text{Eu}$	515 811	6.772	0.423	2.565	515 806	6.7518	0.4150		515 808			264
${}^{153}\text{Eu}$		17.37	0.401							31.5	0.24	
${}^{151}\text{Eu}$	515 745	6.70	0.294	2.576								201
${}^{153}\text{Eu}$		17.26	0.293									
${}^{151}\text{Eu}$	515 740	5.89	0.526	2.569								196
${}^{153}\text{Eu}$		15.13	0.516									
${}^{151}\text{Eu}$	515 693	6.84	0.314	2.545	515 691	7.177	0.308					149
${}^{153}\text{Eu}$		17.41	0.328									
${}^{151}\text{Eu}$	515 688	7.13	0.00									144
${}^{151}\text{Eu}$	515 658	4.396	0.823	2.523	515 667	4.407	0.823		515 668			124
${}^{153}\text{Eu}$		11.09	0.844							16.9	0.31	
${}^{151}\text{Eu}$	515 571	8.06	0.00									27
${}^{151}\text{Eu}$	515 554	7.45	0.00	2.554	515 554	7.45	0.00	2.554		8.162 ^a	0.115 ^a	10
${}^{153}\text{Eu}$		19.03	0.00			19.03						
${}^{151}\text{Eu}$	515 477	7.38	0.00	2.553								-67
${}^{153}\text{Eu}$		18.84	0.03									

^aDeduced from ODNQR data shown in Fig. 3.

reported below.) There is no indication at all of a linear variation through the origin here. There is far more scatter compared even with Fig. 1. This would be consistent with the fact that the calculated lattice contribution, P_{latt} , is much less significant for $P({}^7F_0)$ than for $P({}^5D_0)$.

The better trend (though not good) in the excited state compared with the ground state may indicate that at least some of the sites are explained by the distortion model, though there are more sites that could not be explained. Table III lists the excited state quadrupole parameters and the growth origin of the particular defect sites that show potential consistency with this model; these could possibly be worth studying from this point of view.

Another factor in the Hamiltonian potentially capable of explaining the transition energy shifts among the defect sites with the change in environment is the free-ion contribution described by the Slater parameters. The observed differences between the free-ion energy levels and the baricenters of crystal-field-split J levels in crystals—typically as large as 50 cm^{-1} —have long been attributed to a modification of the Slater parameters by the effects of covalency in the crystal

environment.⁹ As a test of this idea, Newman¹⁰ calculated the magnitude of changes expected due to covalency in the system $\text{Pr}^{3+}:\text{LaCl}_3$, and concluded that this would *not* account for the observed changes, but then went on to show that a modification to the local dielectric constant was in principle a more likely candidate. In the present case the dielectric constant model—which implies a uniform dielectric continuum—seems inappropriate as a description of a single defect site, but the physical consequences of the *polarizability* of atoms local to the defect site would presumably be the same. Another indication of environmental sensitivity is given by the comparison of the $\text{Eu}^{3+} {}^5D_0$ - 7F_0 energy for different crystal hosts, as shown in Table IV. Even if the CaF_2 result is ignored this is still an energy range $\sim 150 \text{ cm}^{-1}$, well in excess of the defect site range in EuVO_4 . As a further test, measurements were made of the variation of the 5D_1 - 7F_0 and 5D_2 - 7F_0 energies with Eu concentration in the system $\text{Eu}:\text{YVO}_4$.¹¹ Over the range 0.5–100% the observed variation was linear with concentration and equal to $\sim 10 \text{ cm}^{-1}$ between the extremes. The EuVO_4 lattice constant is greater than that of YVO_4 , so that the

TABLE III. Relationship between the quadrupole interaction and the energy shift in the 5D_0 state for ${}^{153}\text{Eu}$, for those lines corresponding to the predictions of the “distortion” model. P is the quadrupole interaction parameter (MHz), η is the asymmetry parameter, and δE is the energy difference (GHz) between the defect and intrinsic site 7F_0 - 5D_0 transitions.

Growth	Frequency (GHz)	δE (GHz)	P	η	$P^2(1 + \eta^2/3)/\delta E$
A	515 691	146.7	25.7	0.1	4.50
D	515 723	178.5	25.6	0.67	4.21
G	515 802	257.8	31.7	0.29	4.01
D	515 808	263.6	32.3	0.24	4.02
G	515 810	266.0	31.9	0.58	4.25
L	515 858	314.0	31.1	0.77	3.70
G	515 863	319.4	20.5	0.67	3.76
I	515 864	320.0	35.8	0.55	4.40
L	516 079	534.5	47.8	0.37	4.47
D	516 081	537.0	45.8	0.19	3.95
G	516 212	667.5	47.5	0.64	3.83

observed shift to higher energy correlates with the increasing size of the Eu^{3+} environment. Additional evidence of this was also obtained from a study of 5D_J levels in $\text{Eu}^{3+}:\text{RVO}_4$ ($R = \text{Eu}, \text{Gd}, \text{Tb}, \text{Dy}, \text{Y}, \text{and Lu}$), where again shifts to higher energy correlate with unit cell size. The details of these studies have been presented elsewhere.¹¹ This leads to the hypothesis that *higher* energy Eu^{3+} defect sites are generally those either near vacancies or near impurities with radii *smaller* than those of normal ions, in which case lattice deformations give *more* space around the Eu^{3+} ion, and vice versa: *lower* energy Eu^{3+} defect sites are generally those either near interstitials or near impurities with radii *larger* than those of normal ions, in which case lattice deformations give *less* space around the Eu^{3+} ion. This is qualitatively consistent with the known presence of Pb^{4+} as an impurity in these flux-grown crystals (its ionic radius is smaller than that of Eu^{3+}) and with the obvious bias of the entire defect spectrum to the high energy side of the intrinsic site energy. The “fluorine” lines at 516 389, 516 415, and 516 635 GHz (17 224.88, 17 225.75, and 17 233.09 cm^{-1} , respectively), thought to be present only in crystals grown with fluxes containing fluorine, also fit into this scheme well, since F^- has a smaller ionic radius than O^{2-} , which it replaces in the lattice, perhaps with the help of a charge compensating electron.

In a further effort to identify the origin of specific defect lines, a number of growths were prepared with intentional rare earth impurities and with the expectation that Eu^{3+} defect sites might form preferentially adjacent to the dopant

ions. This mechanism for defect formation would be indicated by increased optical intensities of those defect lines or by a difference in the hole burning dynamics of those defect lines. It was difficult to observe holes in all of the defect sites of growths $H(1.5\% \text{Sm}^{3+})$, $J(1\% \text{Ho}^{3+})$, and $K(1\% \text{Dy}^{3+})$. For growth $E(\text{GdVO}_4:1\% \text{Eu}^{3+})$ no holes could be observed for any sites. The impurity ions or stoichiometric Gd^{3+} ions were very effective in promoting rapid Eu^{3+} nuclear spin relaxation. Since all lines in a particular doped growth seemed to be similarly affected, one can conclude that magnetic dipolar interaction—which is long-range—is the dominant mechanism in the relaxation process. The observation of holes involves a competition between hole burning rate and hole relaxation. The time scale of the present experiments was 200 ms or longer, and it may be worthwhile to repeat these experiments using two lasers to independently burn and read or to use a fast scanning technique to read short-lived holes.

For the different nondoped growths it was noted that, in general, the purer the crystal the easier it was to burn holes. This is consistent with the expectation of longer hole lifetime as impurity-induced relaxation is eliminated. Thus growth A (pure) was found to contain very many easily burnable lines in contrast to growth G (excess Pb), again consistent with the view that paramagnetic impurities were highly effective in promoting Eu^{3+} nuclear spin relaxation. Also, for all growths it was noted that all defect lines *below* the energy of the intrinsic line were either difficult or impossible to burn. These data are of particular interest in connection with energy transfer processes, which are to be addressed in a further paper.

TABLE IV. $\text{Eu}^{3+} {}^7F_0$ - 5D_0 energy in various hosts.

Hosts	Energy (cm^{-1})
CaF_2 (G1 center)	17 430
LaF_3	17 293
EuF_3	17 290
LaCl_3	17 267.35
$\text{Eu}(\text{OH})_3$	17 225
EuAsO_4	17 215
EuVO_4	17 196.7
$\text{Y}_2\text{O}_2\text{S}$	17 143.3

V. OPTICALLY DETECTED NUCLEAR QUADRUPOLE RESONANCE (ODNQR) EXPERIMENTS

To complement hole burning experiments that provided (P, η) values for the 5D_0 excited state, we turned to ODNQR which produces (P, η) data for the 7F_0 ground state. In addition, ODNQR data is some two orders of magnitude more precise than hole burning data, allowing far more stringent tests of identity between defect sites in differ-

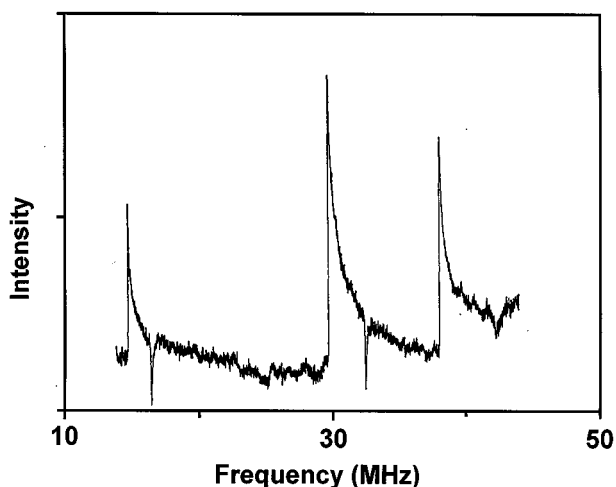


FIG. 3. The ODNQR spectrum for the 515 554 GHz line, showing both ground and excited state resonances in the frequency range 15–45 MHz. The upward pointing peaks, corresponding to stronger fluorescence, are the nuclear resonances in the ground state (7F_0). The downward pointing peaks, corresponding to less fluorescence or stronger holeburning, are the resonances of the optically excited state (5D_0).

ently prepared EuVO_4 growths and a much more precise determination of other parameters that would be needed for a more detailed defect site analysis.

In ODNQR experiments the hole burning setup is augmented by the addition of radio frequency (rf) equipment and a crystal mount that allows simultaneous optical and rf irradiation at 1.5 K. The technique is identical to that used in a variety of double-resonance experiments, and a preliminary report of analyses of a few defect site lines in EuVO_4 has been published.^{4,12}

The present work uses basically the same setup but with refinements at nearly all stages. The crystal was mounted in a 5 mm diameter 5-turn rf coil of 22 gauge wire connected to the center conductors of incoming and outgoing coaxial cables. The coil was designed to act as a transmission line over the range 5–80 MHz by mounting 11 pF capacitors from each of the coil turns to ground. Optical excitation and hole burning was achieved as before by an Ar^+ laser pumped CR599-21 dye laser, and the resulting fluorescence was picked up by an optical fiber bundle and sent to a McPherson 218 monochromator tuned to the 5D_0 - 7F_2 fluorescence emission wavelength. The signal was amplified by a Tektronix 7A22 amplifier in a 7904 oscilloscope and sent to an analog-to-digital converter. The computer-controlled PTS500 rf synthesizer output was sent to the coil after being amplified by an ENI 411LA rf power amplifier. The transmission line including the coil was terminated by a 50 Ω load. The rf magnetic field in the coil was ~ 4 G and the rf was swept at a rate of 17 ms per data point (10 to 20 kHz per point).

Figure 3 shows the result of a frequency scan for a particular defect line over a wide range (10 to 50 MHz). The rf absorption peaks were found to be asymmetric, and a detailed investigation confirmed the conclusions drawn in previous work,⁴ that the asymmetry is a consequence of the dynamics of the double-resonance process, and that a truly

symmetrical lineshape can be detected by a procedure that takes such factors into account. Reversing the direction of the frequency sweep gave exactly the same ODNQR frequency and the tail of the peak was on the lower frequency side. Slowing down the sweep rate also resulted in more symmetric line shapes. On sites that are easier to burn, the peaks were more symmetric. It should be noted that Fig. 3 displays both ground and optically excited state resonances. It was usually found to be more difficult to detect the latter.

Table II collates data believed to relate to the same defect lines in each of the three sets of experiments: the ODNQR experiments carried out on growth A and the Oak Ridge National Laboratory (ORNL) EuVO_4 crystals—which yield data for the 7F_0 ground state—together with growth A hole burning experiments that yield data for the 5D_0 excited state. In this latter case these data are a small fraction of the 5D_0 data displayed in Fig. 1, and are included here to allow a comparison of (P, η) for both the ground and excited states. The ORNL crystals were prepared quite separately from all the other crystals, as a further test of the role of growth conditions. The comparatively high precision in the two sets of ODNQR data allows a detailed assessment of just how identical the particular defect sites are in the two different crystal growths. Not all defect lines were amenable to a complete analysis, hence there are occasional gaps in the table.

The ratio (${}^{153}\text{P}/{}^{151}\text{P}$) is listed for each of the ODNQR datasets in Table II, and can be seen to be close to the value 2.54, the ratio of the respective nuclear quadrupole moments. This implies that pseudoquadrupolar effects in EuVO_4 are very small for nearly all the defect sites, which is somewhat surprising since such effects are expected to be more important in the 7F_0 ground state due to the relative proximity of the $J=2$ excited state.^{7,8,13–19} A related effect is the difference in the values of η for the two isotopes ${}^{151}\text{Eu}$ and ${}^{153}\text{Eu}$, which with ODNQR precision is seen to be significant for some of the lines listed. There has been much discussion of such additional mechanisms in relation to Eu systems displaying large pseudoquadrupolar effects,⁸ and Table V lists data published by other authors for a variety of Eu^{3+} environments.^{7,13–19} The relative insignificance of pseudoquadrupolar effects implied by these results could mean that EuVO_4 is a relatively simple system, with few if any additional unknown mechanisms not properly taken account of in the original Hamiltonian. However, discussions presented in Sec. VI show that there may be additional quadrupole interaction mechanisms in the ground state that are not well understood.

Another issue raised by Table II is the identity of frequency in the two ODNQR data sets. On occasion the optical frequencies of lines judged to be identical because of the very close agreement of their (P, η) values may differ by as much as 9 GHz, well outside the experimental uncertainty. Also, the reverse situation obtains, for example in the case of the growth A 515 693 GHz line which differs from the ORNL 515 691 GHz line by only 2 GHz, yet the values of P differ by 5%. This is a dramatic indication of the sensitivity of the ODNQR technique to very small defect site differences.

It is worth pointing out that the analysis of the observed SHB or ODNQR spectrum depends on the interpretation of its resonance peaks in terms of the quadrupole splittings in

TABLE V. Quadrupole moment ratios $^{153}P/^{151}P$.

Host	Ratio	Method	Reference
CaF ₂ (7F_0)	2.5445±0.0194	Atomic beam	Ref. 13
	2.5835±0.0191	ENDOR	Ref. 14
	2.55±0.34	Optical HFS	Ref. 15
	2.517±0.24	Hollow-cathode discharge	Ref. 16
CaF ₂ C _{3v} (5D_0)	2.553±0.001	ODNQR	Ref. 17, 18
LiYF ₄ (7F_0)	2.564±0.005 ^a	ODNQR	Ref. 19
YAlO ₃ (5D_0)	2.5812±0.0016	ODNQR	Ref. 7
CaF ₂ C _{4v} (7F_0)	2.73	ODNQR	Ref. 18
BaF ₂ C _{4v} (7F_0)	2.75	ODNQR	Ref. 18
EuVO ₄ (7F_0)	2.551±0.006 ^b	ODNQR	This work

^aCorrected for pseudoquadrupole effect.

^bMost sites have the ratio very close to 2.551. The ratios for the ground state of the defect sites range from 2.483 to 2.594.

$I=5/2$ for each of the two isotopes ^{151}Eu and ^{153}Eu . One important criterion is that the sum of the frequencies of the lower two transitions should equal to that of the third transition for each isotope, and the quadrupole moments of the two isotopes should be close to the bare moment ratio of 2.54 (Table V). It is all too easy, with the possibility of overlapping lines and/or some lines being buried in detector noise, to arrive at a totally incorrect result for the parameters (P, η), especially when trying to sort out the antihole spectrum in SHB where the resolution of the spectrum is not nearly as good as ODNQR. The line at 515 979 GHz listed in Table IV is a good example of this, as follows: The earliest hole burning experiments¹ on EuVO₄ were carried out on this line with the hole spectra being analyzed in terms of (P, η) in 5D_0 using the now familiar procedure. However, the data was of sufficient quality that an attempt was made to extract data for the ground state, 7F_0 , from the antihole spectrum—still one of very few occasions on which this has been attempted. In the spectrum, four antihole frequencies can be identified: 16, 26, 40, and 66 MHz. The 26, 40, and 66 MHz antiholes were identified as the three transitions related to ^{153}Eu . To identify the spectrum of ^{151}Eu , it was assumed that there was a 10 MHz transition buried in the wing of the strong central hole, and that the 26 MHz antihole was degenerate, giving three ^{151}Eu antihole resonances at 10, 16, and 26 MHz. These gave the results for 7F_0 :

$$^{151}\text{Eu}: P=4.2\pm 0.1 \text{ MHz}, \quad \eta=0.5\pm 0.1,$$

$$^{153}\text{Eu}: P=10.6\pm 0.1 \text{ MHz}, \quad \eta=0.5\pm 0.1.$$

It was not until the present analysis of the 515 979 GHz ODNQR spectra for both growth *A* and the ORNL crystals was carried out that this earlier analysis could be seen to be wrong. In the ODNQR spectrum, we found resonances at 15.84, 26.32, 39.86, 42.16, and 66.24 MHz. No resonance at around 10 MHz was seen. The three resonances at 15.84, 26.32, and 42.16 MHz belonged to ^{151}Eu . The resonances for ^{153}Eu were less certain. The combination of the 26.32, 39.86, and 66.24 MHz resonances seemed to be promising since the first two added up to 66.18 MHz, very close to 66.24 MHz; but the precision of the experiments was high enough, and the linewidth of the resonances narrow enough

that this was deemed unacceptable. Also against this interpretation was that the calculated quadrupole moment ratio for the two isotopes would have been 1.66, far too different from 2.54. The final interpretation was that the resonances at 39.86 and 66.24 were the lower two transitions for ^{153}Eu , and the third transition expected at 106.10 MHz was not seen due the frequency response of the experimental setup. The results are listed in Table IV.

With hindsight, it is quite obvious that the 40 MHz antihole in the hole burning spectrum covered both the 39.86 and 42.16 MHz resonances. Since even the ODNQR spectrum gave rise to some confusion at this line, the earlier work¹ had little if any chance—at its much lower level of precision—of distinguishing between the original and the correct analyses.

We have shown in earlier work³ that the spectra for growths *A* and *D*—the highest purity EuVO₄ crystals—differ markedly from all other crystal growths (*G–L*), in that they display no defect lines above 516 081 GHz. (This was also true of the ORNL crystals.) Table VI focuses attention on the three prominent defect lines that occur to higher frequencies than this, in all the other crystal growths: at 516 389, 516 415, and 516 635 GHz, in particular, those studied in growth *I* EuVO₄ crystals. It is thought that these lines could be related to the presence of F[−] impurity ions, on the grounds that the flux used in all the crystal growths *G–L* had contained KF, either as a deliberate flux component or as an impurity. As for the analysis of the 515 979 GHz line discussed in the previous paragraph, the 516 635 GHz line presents a similar problem: in this case, we observe four resonances at 11.56, 23.12, 29.35, and 58.33 MHz. This presents a potential ambiguity: either these are the only allowed transitions of an $\eta=0$ system in which the third transition is forbidden; or these are all the transitions of an $\eta=1$ system in which the lower two transitions are degenerate. Our Zeeman ODNQR experiments to be reported later have answered this question. We do indeed have an $\eta=0$ system in 7F_0 for this line. It is also worth pointing out that for this line, the upper state asymmetry parameter η is 0.43.

VI. ELECTRONIC VS LATTICE CONTRIBUTIONS IN 7F_0

Based on the full derivation of the quadrupole interaction Hamiltonian given in Appendix A, we have calculated above

TABLE VI. Results of ODNQR (7F_0) and hole burning (5D_0) experiments on the high energy lines in the growth *I* crystal. P is the quadrupole interaction parameter (MHz) and η is the asymmetry parameter. All P 's listed are in absolute magnitude. These sites were not observed in growth *A* and ORNL samples and are thought to be related to the presence of F^- in the growth flux.

	Freq. (GHz)	7F_0		5D_0	
		P (MHz)	η	P (MHz)	η
${}^{151}\text{Eu}$	516 389	7.113	0.436	19.6	0.13
${}^{151}\text{Eu}$	516 415	5.86	0.18		
${}^{153}\text{Eu}$		14.84	0.20	41.4	0.52
${}^{151}\text{Eu}$	516 635	5.77	0	16.5	0.43
${}^{153}\text{Eu}$		14.59	0.07	42.4	0.44

that for 5D_0 $P_{\text{latt}}/P_{4f}^2 = -29$ and for 7F_0 $P_{\text{latt}}/P_{4f}^2 = -1.8$; that is, the lattice contribution is expected to dominate the 5D_0 excited state, but not the 7F_0 ground state. Table IV lists seven defect lines with (P, η) data for both states, which allows a calculation of the relative importance of P_{latt} and P_{4f}^2 in 7F_0 , if we assume that for a particular Eu isotope the ratio

$$\frac{P({}^5D_0)}{P({}^7F_0)} \cong \frac{P_{\text{latt}}}{P_{\text{latt}} + P_{4f}^2}.$$

Table VII lists these ratios for the seven lines in Table IV, and the 516 635 GHz line listed in Table V. Published data

for other systems are also listed to illustrate the differences.^{8,17-27} Except for very few cases (the fluorides^{17,18,20,23}), the relative signs of $P({}^5D_0)$ and $P({}^7F_0)$ are unknown; thus two values for the ratios are listed as the result of the two possibilities $P({}^5D_0)/P({}^7F_0) > 0$ or < 0 . When the opposite signs are assumed, the electronic contributions cannot be neglected in the 5D_0 state. The values in Table VII have taken that contribution into account for the upper state.

In Table VII it can be seen that the values of P_{latt}/P_{4f}^2 vary widely (-1.53 to -11.5) when the two terms have the same sign, but are more closely scattered over the range -0.553 to -0.878 when the signs are opposite. It should

TABLE VII. Comparison of the ground state and excited state quadrupole interactions. Ratios of the lattice and electronic contributions for 7F_0 are calculated assuming same and opposite signs for the ground and excited states.

Frequency (GHz)	$P({}^7F_0)$ (MHz)	$P({}^5D_0)$ (MHz)	$P({}^5D_0)/P({}^7F_0)$	Same sign P_{latt}/P_{4f}^2	Opposite sign P_{latt}/P_{4f}^2	${}^{151}\eta/{}^{153}\eta$
515 554 (${}^{151}\text{Eu}$)	7.45	8.162	1.096	-11.5	-0.553	
515 868 (${}^{153}\text{Eu}$)	15.56	17.9	1.15	-7.65	-0.565	0.934
515 658 (${}^{153}\text{Eu}$)	11.09	16.9	1.524	-2.91	-0.629	0.975
515 979 (${}^{153}\text{Eu}$)	17.07	25.8	1.511	-2.96	-0.627	1.000
515 816 (${}^{153}\text{Eu}$)	16.74	27.6	1.649	-2.54	-0.647	1.043
515 811 (${}^{153}\text{Eu}$)	17.37	31.5	1.814	-2.23	-0.667	1.055
516 081 (${}^{153}\text{Eu}$)	15.82	45.8	2.90	-1.53	-0.744	1.04
516 635 (${}^{151}\text{Eu}$)	5.77	16.5	2.866	-1.54	-0.757	
YAlO ₃ ^a (${}^{151}\text{Eu}$)	11.50	22.715	1.975	-2.02	-0.680	
KEu(WO ₄) ₂ ^b (${}^{151}\text{Eu}$)	8	19	2.375	-1.72	-0.723	
CaF ₂ C_{3v} ^c (${}^{151}\text{Eu}$)	+8.21	-22.23			-0.747	
CdF ₂ C_{3v} ^c (${}^{151}\text{Eu}$)	+7.85	-12.9			-0.646	
EuP ₅ O ₁₄ ^d (${}^{151}\text{Eu}$)	6.38	8.0	1.254	-4.94	-0.585	
CaF ₂ C_{4v} ^e (${}^{151}\text{Eu}$)				-1.18		
SrF ₂ C_{4v} ^e (${}^{151}\text{Eu}$)					-0.878	
BaF ₂ C_{4v} ^e (${}^{151}\text{Eu}$)					-0.818	
Y ₂ SiO ₅ ^f (${}^{151}\text{Eu}$, site 1)	12.4	27.3	2.20	-1.83	-0.708	
Y ₂ SiO ₅ ^f (${}^{151}\text{Eu}$, site 2)	14.4	27.7	1.924	-2.08	-0.680	
Y ₂ O ₃ ^g (${}^{151}\text{Eu}$)	9.37	23.3	2.486	-1.67	-0.731	

^aReferences 21, 22, and 19.

^bReference 20.

^cReferences 17 and 23.

^dReferences 8, 21, and 24.

^eReference 18.

^fReferences 25 and 26.

^gReference 27.

perhaps be noted that the first two lines in the table are not exceptions or “bad points” that can be ignored because they are not close to the mean value. This is equally true for the $\text{EuP}_5\text{O}_{14}$ result.^{8,21,24}

In deciding which if either of these sets is likely to be the more valid, it is tempting to choose the “opposite sign” results, not only because they scatter less but also because in the two cases^{17,23} where the absolute sign of P_{4f} has been determined they do turn out to be opposite, with ratios equal to -0.747 and -0.646 , respectively. This however has serious consequences for the screening factors $(1 - \sigma_2)$ and $(1 - R_Q)$, as can be seen by examining the theoretical expression for the ratio P_{latt}/P_{4f}^2 [Eq. (A9)]:

$$P_{\text{latt}}/P_{4f}^2 = -\frac{0.73}{(1 - \sigma_2)(1 - R_Q)},$$

where all the other terms in the full expression take the values given in Appendix A. Obviously this implies that for $|P_{\text{latt}}/P_{4f}^2|$ ratios less than 0.73, these two screening factors are actually negative. This was noted by the authors of the -0.747 result above,^{17,23} who argued that their result (the theoretical limit in their case being -0.75 , due to a greater ${}^7F_2 - {}^7F_0$ energy difference) was consistent with the known uncertainties in the two quantities R_Q and σ_2 ; that is, that each of them could conceivably be zero in an extreme situation.

From the larger data set in Table VII it is clear however that nearly half the “opposite sign” ratios are considerably less than $|-0.73|$, implying negative values for $(1 - \sigma_2)$ and $(1 - R_Q)$, which on physical grounds seems rather unlikely. We therefore return to the same sign data set, seeking an explanation for the wide variation in the P_{latt}/P_{4f}^2 ratio shown there.

For YAIO_3 (Ref. 7) the ratio -2.03 was shown to be consistent with a calculation based on the known second order crystal-field parameters and is therefore good evidence for the validity of a “same sign” choice. In that work it was remarked that ratios different from -2.03 would be evidence, in low symmetry sites, that nuclear quadrupolar and crystal-field axes were not coincident, and it is perhaps in this direction that further analysis of the data in Table VII needs to go. The defect sites in EuVO_4 are usually, though not always, of low symmetry, where on symmetry grounds it can be argued that the principal axes will in general be in different directions for the nuclear quadrupole moment, the nuclear Zeeman magnetic moment, and the magnetic properties of all electronic excited states also. Nevertheless, this cannot be the complete, albeit qualitative, explanation for the variation seen in Table VII. The 515 554 GHz defect, for instance, which has a “same sign” ratio equal to -11.5 , is shown in Table IV to have $\eta=0$ to high accuracy, implying accurately axial symmetry in which at least some of the principal axes in the system would coincide. Further work,¹¹ in which angle-dependent ODNMR has been used to determine the principal axes of the nuclear quadrupole and nuclear magnetic moments, is an essential next step in attempting to resolve these major questions.

The pseudoquadrupole interaction is not strong in the present system. The indication of this is the ratio $P({}^{153}\text{Eu})/P({}^{151}\text{Eu})$, which however in Table IV can be seen

to be within 2% of the quadrupole moment ratio (2.54) for the defect lines listed; that is, one would not expect large pseudoquadrupolar effects on these grounds. The same is true for the ratio ${}^{151}\eta/{}^{153}\eta$ listed for the defect lines in Table VII, where the ratio is seen to be within $\sim 5\%$ of unity in all cases. Indeed, for the particular defect line 515 979 GHz already discussed, this ratio is unity to within the accuracy of measurement ($1:10^3$) which is remarkable since the pseudoquadrupolar contribution due to the cross term between the quadrupole interaction and the second order crystal-field terms is bound to be nonzero. For some reason, its effect for this particular defect line is very small indeed, and clearly fails to provide an explanation for the large electronic contribution in the ground state.

VII. CONCLUSION

The primary characteristics of the many defect sites in stoichiometric single crystal europium vanadate, EuVO_4 , have been surveyed. Crystals from a variety of growths have been studied by fluorescence excitation, fluorescence spectroscopy, and by the much higher resolution techniques of hole burning and ODNQR. A number of the defect sites appear at the same optical frequencies (with GHz precision) in different crystal growths, and the nuclear quadrupole splittings that characterize the local Eu^{3+} environment are also remarkably similar in different crystal growths. This makes it possible that these defects are intrinsic to the EuVO_4 structure. Identification of particular defect sites in terms of the spatial arrangement of neighboring atoms is still the major challenge. For example, some of the higher energy defect sites appear to be associated with fluorine. These problems are being addressed using the techniques of time-resolved spectroscopy and Zeeman ODNQR and will form the subject of further publications.

The electronic contribution to the quadrupole interaction in the ground state is larger than the lattice contribution for all sites studied in this work. This conclusion can be extended further to all Eu^{3+} in all crystals studied heretofore, except the special case of the $\text{CaF}_2 C_{4v}$ center where the pseudoquadrupole interaction is strong and no conclusion can be drawn. Using the current quadrupole Hamiltonian, it seems that the electronic shielding parameters R_Q and σ_2 should be negative in these crystals. To this extent, we believe that the current Hamiltonian is not adequate for the description of the ground state, possibly because the principal axes of the lattice and electronic interactions are not necessarily coincident at these low-symmetry (defect) sites.

ACKNOWLEDGMENTS

This research was supported in part by the U.S. Air Force Office of Scientific Research (Grant No. F49620-93-1-0530DEF), NASA (Grant No. NCCW0058), the National Science Foundation (Grant No. OSR-9350546), NATO (CRG 910031), NSF/MONTS, Research Corp, Montana Space Grant Consortium NASA Grant No. NGT40041, the UK Engineering and Physical Science Research Council (Grants No. GR/H50302 and No. GR/H59026), and the U.S. DOE (Contract No. DE-AC05-84OR21400). One of us

(Y.S.) wants to thank R. S. Meltzer for beneficial discussions.

APPENDIX A: THE ELECTRIC QUADRUPOLE INTERACTION

Basic consideration of the electrostatic interaction between the nuclear and $4f$ electron distributions on a rare earth ion leads to the quadrupole interaction Hamiltonian having the form:²⁸

$$H_Q = \frac{eQ}{4I(2I-1)} \left[\langle V_{zz} \rangle \{3I_z^2 - I(I+1)\} + \frac{1}{2} \langle V_{xx} - V_{yy} \rangle (I_+^2 + I_-^2) \right]. \quad (\text{A1})$$

Here

$$e \langle V_{zz} \rangle = \frac{1}{2} \frac{\partial^2}{\partial z^2} \left[-\frac{e}{4\pi\epsilon_0 r} \right]$$

is directly related to the tensor component B_0^2 , with the convention that off-diagonal components of the electric field gradient are eliminated by a suitable choice of quadrupolar tensor axes, and diagonal components are ordered such that

$$|V_{zz}| \geq |V_{yy}| \geq |V_{xx}|.$$

Using Laplace's equation ($V_{xx} + V_{yy} + V_{zz} = 0$) it is also conventional to define the asymmetry parameter η by

$$\eta \langle V_{zz} \rangle = \langle V_{xx} - V_{yy} \rangle. \quad (\text{A2})$$

The nuclear quadrupole moment, Q , is conventionally defined as

$$Q = \langle I, m_I = I | \sum_j (3Z^2 - R^2) | I, m_I = I \rangle, \quad (\text{A3})$$

where the sum is over all the nucleons, and the quantity e^2Q is the quadrupole coupling constant. If a further constant P is defined such that

$$P = \frac{3eQ \langle V_{zz} \rangle}{4I(2I-1)},$$

then the Hamiltonian finally becomes:

$$H_Q = P \left\{ I_z^2 - \frac{I(I+1)}{3} + \frac{\eta}{6} (I_+^2 + I_-^2) \right\}. \quad (\text{A4})$$

The value of P depends linearly on the magnitude of $\langle V_{zz} \rangle$, the total local electric field gradient, whatever its origin.

To obtain an effective nuclear spin Hamiltonian, one makes an explicit perturbation calculation with real J -mixed electronic states 7F_0 or 5D_0 . Separate contributions to P arise from the $4f$ electrons surrounding the nucleus (P_{4f}) and from the ions in the surrounding crystal lattice (P_{latt}). From the above derivation we can write expressions for P_{4f} in the formalism of Stevens operator equivalents as well as tensor operators. The first-order contribution P_{4f}^1 becomes

$$\begin{aligned} P_{4f}^1 &= \frac{3e^2Q}{4I(2I-1)} \frac{1}{4\pi\epsilon_0} \langle r^{-3} \rangle (1-R_Q) \langle J | \alpha | J \rangle \\ &\quad \times \langle 3J_z^2 - J(J+1) \rangle \\ &= \frac{3e^2Q}{2I(2I-1)} \frac{1}{4\pi\epsilon_0} \langle r^{-3} \rangle (1-R_Q) \langle J | C_0^2 | J \rangle. \end{aligned} \quad (\text{A5})$$

For both 5D_0 and 7F_0 this contribution is zero, so we further consider the *second-order* contribution P_{4f}^2 , the cross term arising between the crystal field and the quadrupole interaction:

$$P_{4f}^2 = \frac{6e^2QB_0^2}{2I(2I-1)} \frac{1}{4\pi\epsilon_0} \langle r^{-3} \rangle (1-R_Q) \frac{\langle 2 | C_0^2 | 0 \rangle^2}{(E_2 - E_0)}. \quad (\text{A6})$$

For Eu the accepted values¹⁹ of the constants in the above equation are $Q({}^{153}\text{Eu}) = 2.42$ barns, $\langle r^{-3} \rangle_{4f} = 50 \text{ \AA}^{-3}$, $(1-R_Q) = 0.8$, and the matrix element $\langle 2, 0 | C_0^2 | 0, 0 \rangle = 0.1049$ for states in 5D , and 0.2024 in 7F , using wave functions in intermediate coupling.^{19,29} Using $E({}^5D_2) - E({}^5D_0) \cong 4200 \text{ cm}^{-1}$, $E({}^7F_2) - E({}^7F_0) \cong 1000 \text{ cm}^{-1}$, the above expression yields

$$P_{4f}^2({}^5D_0) = 2.6 \times 10^{-3} B_0^2 \text{ MHz},$$

$$P_{4f}^2({}^7F_0) = 4.1 \times 10^{-2} B_0^2 \text{ MHz}.$$

Next we consider the lattice contribution, P_{latt} , arising from the neighboring ions in the crystal lattice:

$$P_{\text{latt}} = \frac{3eQ \langle V_{zz}^l \rangle}{4I(2I-1)},$$

where $\langle V_{zz}^l \rangle$ describes the electric field gradient produced by the surrounding ions: that is, $e \langle V_{zz}^l \rangle = 2B_0^2 / \langle r^2 \rangle$. Allowing for the Sternheimer shielding parameters,³⁰

$$P_{\text{latt}} = \frac{3Q}{2I(2I-1)} \frac{B_0^2}{\langle r^2 \rangle} \frac{(1-\gamma_\infty)}{(1-\sigma_2)}. \quad (\text{A7})$$

Using accepted values,¹⁹ $(1-\gamma_\infty) = 81$, $(1-\sigma_2) = 0.5 \pm 0.1$, and $\langle r^2 \rangle_{4f} = 0.233 \text{ \AA}^2$, the above equation yields

$$P_{\text{latt}} = -7.56 \times 10^{-2} B_0^2 \text{ MHz}.$$

The relative importance of the lattice and electronic contributions can be expressed by the ratio of Eq. (A7) and Eq. (A6)

$$\frac{P_{\text{latt}}}{P_{4f}^2} = \frac{4\pi\epsilon_0(E_2 - E_0)(1-\gamma_\infty)}{2 \langle r^{-3} \rangle (1-R_Q) \langle r^2 \rangle (1-\sigma_2) \langle 2 | C_0^2 | 0 \rangle^2}. \quad (\text{A8})$$

Putting in various constants used above, and keeping R_Q and σ_2 as parameters since they are less certain, we have for the ground state 7F_0 :

$$\frac{P_{\text{latt}}}{P_{4f}^2} = \frac{0.73}{(1-R_Q)(1-\sigma_2)}. \quad (\text{A9})$$

This perturbation analysis also gives rise to both lattice and $4f$ contributions to the asymmetry parameter η . From the earlier definition (Eq. A2), we obtain

$$\eta_{\text{latt}} = \frac{B_2^2(C_2^2 + C_{-2}^2)}{B_0^2 C_0^2} = \sqrt{6} \frac{B_2^2}{B_0^2}. \quad (\text{A10})$$

There are additional contributions to η involving the P_{4f}^2 terms, and these cannot be simply added to P_{latt} . However, it turns out that the effect of these contributions to η is negligible so long as the crystal-field splittings in 7F_2 are negligible compared with the ${}^7F_2 - {}^7F_0$ energy difference.

Pseudoquadrupole effects

The terms other than P_{latt} and P_{4f} are known as *pseudoquadrupole* contributions, since they have the same form as the original quadrupole term but have a different physical origin (such as second order effects of the magnetic hyperfine interaction). Usually, they are much smaller than the ‘‘true’’ quadrupole terms.

For the singlet Eu^{3+} ground state the total electronic angular momentum is nominally $J=0$. One consequence of this is that the hyperfine interaction $\mathbf{A}\mathbf{I}\cdot\mathbf{J}$ has zero effect in first order. In *second* order however the hyperfine interaction appears in a cross term both with itself and with the Zeeman interaction $H = -\mathbf{B}\cdot\boldsymbol{\gamma}\cdot\mathbf{I}$, while the quadrupole interaction appears in a cross term with the second-order terms in the crystal field. This leads to an effective Hamiltonian of the form^{31–33}

$$H = -\mathbf{B}\cdot\boldsymbol{\gamma}\cdot\mathbf{I} + P \left\{ I_z^2 - \frac{I(I+1)}{3} + \frac{\eta}{6} (I_+^2 + I_-^2) \right\}.$$

Here the magnetogyric tensor $\boldsymbol{\gamma}$ is defined by

$$\gamma_{ii} = -(g_I \mu_B + 2g_J \mu_B \Lambda_{ii}), \quad (i=x,y,z)$$

with

$$\Lambda_{ii} = \sum_n \frac{A_i |\langle 0 | J_i | n \rangle|^2}{E_n - E_0}.$$

P now includes a pseudoquadrupole term:

$$P_a = A_J [(\Lambda_{xx} + \Lambda_{yy})/2 - \Lambda_{zz}],$$

giving a total P :

$$P = P_a + P_{\text{latt}} + P_{4f}^1 + P_{4f}^2.$$

APPENDIX B: THE RELATIONSHIP BETWEEN (P, η) AND (A, B)

For a nuclear spin $I=5/2$ the quadrupole Hamiltonian in zero field produces three Kramers’ doublets whose energies

are best described by the differences (A, B) between the lowest-middle and middle-upper states, respectively. It can easily be shown that the corresponding Hamiltonian matrix in zero field reduces to the following eigenvalue equation for the case $I=5/2$:

$$x^3 - (336 + 112\eta^2)x - 1280(1 - \eta^2) = 0,$$

where

$$x = 6\lambda/P,$$

and $\lambda_{1,2,3}$ are the energy eigenvalues of the matrix. It is possible to solve this cubic equation by the use of a trigonometric substitution. If an intermediate variable θ is defined such that

$$\theta = \frac{1}{3} \arccos \left\{ \frac{-10(1 - \eta^2)}{\sqrt{7^3(1 + \eta^2/3)^3}} \right\}$$

then the three real roots are given by

$$x_n = -8\sqrt{7(1 + \eta^2/3)} \cos \left(\theta + \frac{2n\pi}{3} \right),$$

where $n=0,1,2$. It is possible to demonstrate that for all cases $n=2$ corresponds to the middle state, while $n=0,1$ correspond to the upper and lower states, respectively. The following energy differences can therefore be defined:

$$A + B = P(x_1 - x_0)/6,$$

$$B = P(x_2 - x_0)/6,$$

$$A = P(x_1 - x_2)/6.$$

Hence the ratio of *measured* energy differences is $r = B/A$, where $1 \leq r \leq 2$. After some manipulation this reduces to

$$r = 2[\sqrt{3} \cot \theta - 1].$$

By simply measuring the ratio of the energy splittings for a given isotope from hole burning data it is possible to derive a single, unique value for θ and hence for η . The overall splitting $\delta = A + B$ can be used to calculate the value of P :

$$P = \frac{3\delta}{4\sqrt{21(1 + \eta^2/3)} \sin \left(\theta + \frac{\pi}{3} \right)}.$$

The computer program used to calculate the parameters (P, η) from the two quadrupole splittings (A, B) could also work in reverse, to produce values of (A, B) for a given (P, η) .

¹R. L. Cone, R. T. Harley, and M. J. M. Leask, *J. Phys. C* **17**, 3101 (1984).

²R. L. Cone, M. J. M. Leask, M. G. Robinson, and B. E. Watts, *J. Phys. C* **21**, 3361 (1988).

³R. L. Cone, P. C. Hansen, M. J. M. Leask, and B. M. Wanklyn, *J. Phys.: Condens. Matter* **5**, 573 (1993).

⁴R. L. Cone, P. C. Hansen, and M. J. M. Leask, *J. Opt. Soc. Am. B* **9**, 779 (1992).

⁵L. E. Erickson, *Opt. Commun.* **21**, 147 (1977).

⁶L. E. Erickson, *Phys. Rev. B* **16**, 4731 (1977).

⁷L. E. Erickson and K. K. Sharma, *Phys. Rev. B* **24**, 3697 (1981).

⁸R. M. Macfarlane and R. M. Shelby, in *Spectroscopy of Solids Containing Rare Earth Ions*, edited by A. A. Kaplyanski and R. M. Macfarlane (North-Holland, Amsterdam, 1987), pp. 51–184.

⁹C. K. Jørgensen, *Modern Aspects of Ligand Field Theory* (North-Holland, Amsterdam, 1971).

- ¹⁰D. J. Newman, *J. Phys. Chem. Solids* **345**, 541 (1973).
- ¹¹Y. Sun, Ph.D. thesis, Montana State University, 1993.
- ¹²P. C. Hansen, Ph.D. thesis, Oxford University, 1990.
- ¹³P. G. H. Sandars and G. K. Woodgate, *Proc. R. Soc. London, Ser. A* **257**, 269 (1960).
- ¹⁴J. M. Baker and F. I. B. Williams, *Proc. R. Soc. London, Ser. A* **267**, 283 (1962).
- ¹⁵K. Krebs and R. Winkler, *Naturwissenschaften* **47**, 490 (1960).
- ¹⁶W. Muller, A. Stendel, and H. Walther, *Z. Phys.* **183**, 303 (1965).
- ¹⁷A. J. Silversmith, A. P. Radliński, and N. B. Manson, *Phys. Rev. B* **34**, 7554 (1986).
- ¹⁸A. J. Silversmith and R. M. Macfarlane, *Phys. Rev. B* **45**, 5811 (1992).
- ¹⁹L. E. Erickson, *Phys. Rev. B* **34**, 36 (1986).
- ²⁰A. J. Silversmith and N. B. Manson, *J. Phys. C* **17**, L97 (1984).
- ²¹R. M. Shelby and R. M. Macfarlane, *Phys. Rev. Lett.* **45**, 1098 (1980).
- ²²R. M. Shelby and R. M. Macfarlane, *Phys. Rev. Lett.* **47**, 1172 (1981).
- ²³A. P. Radliński and A. J. Silversmith, *Phys. Rev. B* **34**, 86 (1986).
- ²⁴R. M. Macfarlane, R. M. Shelby, A. Z. Genack, and D. A. Weitz, *Opt. Lett.* **5**, 462 (1980).
- ²⁵R. Yano, M. Mitsunaga, and N. Uesugi, *Opt. Lett.* **16**, 1884 (1991).
- ²⁶R. Yano, M. Mitsunaga, and N. Uesugi, *J. Opt. Soc. Am. B* **9**, 992 (1992).
- ²⁷W. R. Babbit, A. Lezama, and T. W. Mossberg, *Phys. Rev. B* **39**, 1987 (1989).
- ²⁸M. Weissbluth, *Atoms and Molecules* (Academic, San Diego, 1978).
- ²⁹G. S. Ofelt, *J. Chem. Phys.* **38**, 2171 (1963).
- ³⁰R. M. Sternheimer, *Phys. Rev.* **146**, 140 (1966).
- ³¹B. R. Reddy and L. E. Erickson, *Phys. Rev. B* **27**, 5217 (1983).
- ³²K. K. Sharma and L. E. Erickson, *J. Phys. C* **18**, 2935 (1985).
- ³³M. A. Teplov, *Sov. Phys. JETP* **26**, 872 (1968).